Available online at www.sciencedirect.com
ScienceDirect
Ceramics International 37 (2011) 1377–1391
CERAMICS INTERNATIONAL
www.elsevier.com/locate/ceramint

Evaluation of hydroxyapatite and β-tri calcium phosphate microplasma spray coated pin intra-medullary for bone repair in a rabbit model

Arjun Dey [a], Samit Kumar Nandi [b,**], Biswanath Kundu [a,*], Chandrasekhar Kumar [b], Prasenjit Mukherjee [b], Subhasis Roy [b], Anoop Kumar Mukhopadhyay [a], Mithlesh Kumar Sinha [a], Debabrata Basu [a]

[a] Central Glass and Ceramic Research Institute, Council of Scientific and Industrial Research, Kolkata 700032, India
[b] West Bengal University of Animal and Fishery Sciences, Kolkata 700037, India

Received 30 July 2010; received in revised form 18 November 2010; accepted 3 January 2011
Available online 4 February 2011

Abstract

Here we report a comparative study of the healing kinetics of surgically created artificial defects in the tibia of New Zealand white rabbits. Comparison of the healing kinetics was made for uncoated conventional SS316L intramedullary pins, and the same pins with microplasma sprayed (MIPS) pure hydroxyapatite (HAp) and beta-tri calcium phosphate (β-TCP) coatings. After thorough material characterizations including XRD, FTIR, SEM, etc., MIPS coated pins were implanted to such animals. Serum biochemistry, radiology and fluorochrome labelling were used to evaluate the comparative healing kinetics of these implants in vivo. In comparison to those of the uncoated pins, the pins coated with both MIPS HAp and β-TCP showed significant increment of alkaline phosphatase up to 15th postoperative day, insignificant changes in serum phosphorus and calcium with uneventful healing of bone defect. There was development of Havarsian canals and well-defined peripherally placed osteoblasts along with evidence of angiogenesis and comparatively more new bone formation in the defect site. On a comparative scale, the performance of the β-TCP coated intramedullary pins was much better than that of the pure HAp coated pins than the uncoated intramedullary pins.

Keywords: Hydroxyapatite; β-Tri calcium phosphate; Microplasma spraying; In vivo animal trial; Intramedullar pinning; Bone defects healing

1. Introduction

Intramedullary pinning is commonly used fracture fixation technique to provide stability to long bone fractures in animals [1,2]. They are relatively easy to remove after healing of fracture. Amongst other constraints of this technique, some is less stability, resulting in a slower return to limb function and may involve more after-care over other internal fixation techniques. Besides other complications associated with intramedullary pinning, include delayed union or nonunion, excessive flexibility, pin deformation, fatigue fractures or migration. To overcome these, the basic research in the fracture demands essentially to determine the optimum materials, geometry and structural properties of fixation devices.

Implant loosening/migration is an unresolved complication associated with internal fixation. It is generally accepted that this problem may be overcome by modifying the implant/bone interface for improved osseous integration. Improved osseous integration may be obtained by the use of hydroxyapatite (HAp), β-tri calcium phosphate (β-TCP) and their composite coatings. A number of studies has suggested that the effectiveness of calcium phosphate surface coatings, nominally HAp to enhance the osteoconductivity of metallic implant [3–5]. These coatings have been shown to promote osseointegration by stimulating bone growth onto the surface [6]. The problem associated with HAp and Ca–P coatings with thickness of ∼10–100 μm is failure of implant during long-term use, in

* Corresponding author at: Bioceramics and Coating Division, Central Glass and Ceramic Research Institute, 196, Raja S.C. Mullick Road, Post Office: Jadavpur University, Kolkata 700032, India. Tel.: +91 33 24733469x3337; fax: +91 33 24730957.
** Corresponding author at: Department of Veterinary Surgery and Radiology, West Bengal University of Animal and Fishery Sciences, 37 and 68, Kshudiram Bose Sarani, Kolkata 700037, India. Tel.: +91 9433111065; fax: +91 33 25571986.
E-mail addresses: samitnandi1967@gmail.com (S.K. Nandi), biswa_kundu@rediffmail.com (B. Kundu).

0272-8842/$36.00
doi:10.1016/j.ceramint.2011.01.005

either adhesion (delamination) to the implant itself or in internal cohesion of the actual coating [7]. If this happens *in situ*, it may encourage fibrous tissue formation at the implant surface and could result in implant loosening. This along with production costs has induced the search for a coating that encourages good fibrin attachment and bony integration, while being good for adhesion to the implant surface and cohesion within its internal structure.

Microplasma spraying (MIPS) technique [8–13] developed only a few years ago is gaining importance and applied for development of various coatings of metals and metallic alloys [9,12], ceramics and ceramic composites [9,10,13] and also bioceramics e.g. HAp [8,11]. The term ''micro'' generally refers to the comparably low power level than that of the conventional macro-plasma spraying (MAPS) [9]. This spray process utilizes a much lower plasma power (1–4 kW) and much smaller spray spots (3–5 mm) due to its narrow laminar plasma jet compared to those of the conventional MAPS process and provide a higher degree of crystallinity than that provided by MAPS along with very less amount of impurity phase [8]. Coating of intramedullary pins with bioactive ceramics, e.g. HAp, β-TCP, etc. by MIPS could be a solution for this particular fracture fixation technique which can provide stability to long bone fractures [14–16]. Compared to the conventional macroplasma sprayed process, the MIPS process: (a) requires much lesser plasmatron power (e.g. 1–4 kW c.f. 10–40 kW), (b) generally avoids formation of impure and amorphous phases, (c) provides much higher degree of phase purity and crystallinity (e.g. >80% c.f. ≤70%) and (d) induces higher degree of porosity (e.g. ∼20% c.f. ≤2–10%) that facilitates bony tissue in-growth [8,14,16–18]. Over the past few years, HAp and to a much lesser extent, β-tri calcium phosphate (β-TCP) have been successfully applied for porous coating on metallic implants to provide easier in-growth of bony tissues [17,19–21].

Recently, in a significant effort Junker et al. [22] attempted bone fixation using a MIPS calcium phosphate coated titanium (Ti) implant in goat. However, to the best of knowledge, the present work is the maiden report on the comparative healing performance of uncoated intermedullary SS316L pins, and MIPS pure HAp and β-TCP coated intermedullary SS316L pins for bone fixation in New Zealand white breed of rabbit.

2. Materials and methods

2.1. Materials preparation and characterizations

Preparation of HAp and β-TCP powders with Ca/P molar ratios of 1.67 and 1.50 by simple wet chemical routes followed by calcination at 1250 °C and 1200 °C, respectively; led to phase pure, free flowing granule formation [23,24]. Flowability as measured by a Hall flowmeter (Lloyds, India, ASTM B 212 [25]) showed that powder with size range of 53–64 μm gave the best flow properties (∼0.5 g/s). Subsequently, these were used for microplasma spraying [17,20]. Next, rectangular (155 mm × 20 mm × 2 mm and 25 mm × 25 mm × 2 mm) and cylindrical (25.4 mm diameter, length 25.4 mm) stainless steel (SS316L) coupon substrates were microplasma sprayed. Prior to MIPS treatment, the substrates were ground flat parallel and blasted with about 200–250 μm alumina grits to an average centre line average (CLA) of about 2.5 μm (Taylor Hobson I-120, UK). Atmospheric MIPS was carried out using a commercial instrument (Miller Maxstar 200 SD 2.5 kW, USA) at a low plasmatron power of 1.5 kW with external powder feeder chamber. The plasma spray parameters used in the present study for coating on the SS316L substrate are given in Table 1. The coating thus obtained was subsequently annealed at 600 °C for 2 h to modify the coating properties and adherence to the substrate. The phase purity and degree of crystallinity of the coatings were analyzed by X-ray diffraction (XRD; Philips PW 1710, Holland) technique using monochromatic Cu $K_{\alpha 1}$ radiation at 55 mA and 40 kV after following methods given in Klug and Alexander and Landi et al., respectively [26,27]. Percent of phase content for composite phase was calculated by external standard method. The mass absorption coefficients are given in Table 2. For samples containing an amorphous fraction, the percent crystallinity was determined by deducting the sum of all the weight fractions of the crystalline phases in the mixture from 100%.

The infrared (IR) spectrum of the coating was recorded in the mid IR region by a Fourier transformed infra-red spectrometer (FTIR; Perkin-Elmer, Model: 1615, USA). The microstructural characterizations and coating thickness measurements were carried out by scanning electron microscopy (SEM; s430i, Leo, UK), field emission scanning electron microscopy (FESEM; Supra VP35 Carl Zeiss, Germany) and subsequently by an image analyzer (Leica Q500MC, UK).

Table 1
Parameters for MIPS process.

Parameters	Values
Primary gas pressure (Ar)	4 bar at 20 °C
Secondary gas pressure (Ar)	4 bar at 20 °C
Primary gas (plasma gas) flow rate	10 SLPM
Secondary gas (shielding gas) flow rate	20 SLPM
Powder deposition rate	∼1.5 mg/s
Powder size	∼−53 + 64 μm
Input current	∼40 A
Input voltage	∼30 V
Plasmatron power	<1.5 kW
Stand-off distance	75 mm
Rotational speed of sample	150 rpm
Distance between cathode and plasma nozzle	1.7 mm
Distance between anode and plasma nozzle	1 mm

SLPM: standard liters per minute.

Table 2
Mass absorption coefficients of different calcium phosphate phases.

Phase (s)	Mass absorption coefficient
Hydroxyapatite	86.6531
Tri calcium phosphate	95.5864
Calcium phosphide oxide, Ca_4P_2O	135.333
Plasma spray coating consisting of β-TCP, α-TCP and Ca_4P_2O	99.5381

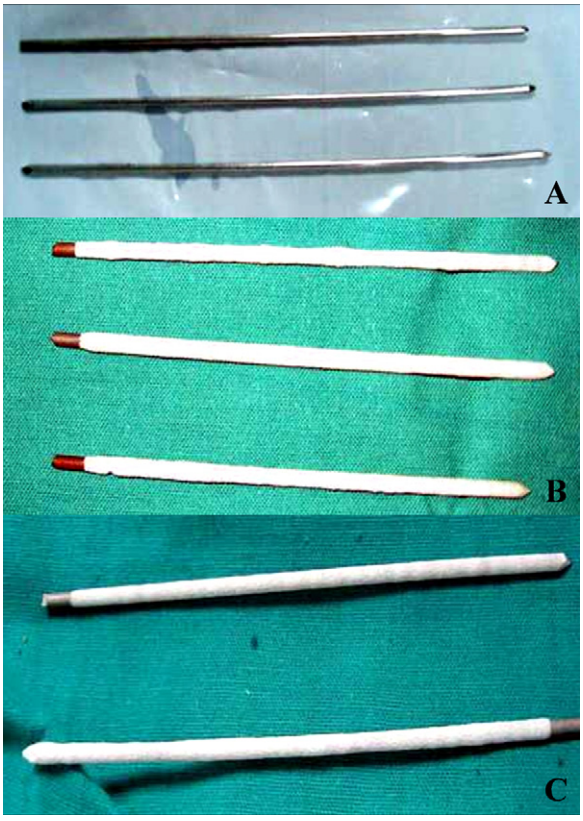

Fig. 1. SS316L Intramedullar pins: (A) uncoated, MIPS, (B) HAp and (C) β-TCP coated.

Samples were sputtered coated with Au–Pd (∼50–70 nm coating thickness) prior inserting in the sample chamber of electron microscopy. Prior to in vivo animal trials, the actual uncoated pins, pins coated by MIPS HAp and β-TCP coating are shown in Fig. 1A, Fig. 1A and Fig. 1C, respectively. The bonding strength of the coatings was evaluated as per ASTM C633 specification using a universal testing machine (Instron 5500 R, USA) [28]. Details of the procedure have been reported elsewhere [11,17,20]. Briefly, MIPS-HAp/β-TCP coatings were put on SS316L cylindrical stubs (25.4 mm diameter and length 25.4 mm) (loading stub, L and the substrate stub, S). The coated stub (S) was joined to another uncoated stub (L) with a commercially available adhesive tape (FM 1000 adhesive film, Cytec Industries Inc., NJ, USA). The tape was made by a mixture of polyamide and epoxy resin with an appropriate curing agent. The stubs were then mounted on a snugly fitted fixture and kept in an oven for about 5 h at 300 °C for curing purpose. Tensile test was carried out at a cross-head speed of 0.1 mm/min. using a Universal Testing Machine (UTM Instron 5500 R, USA) under ambient conditions. The bonding strength of the coating was obtained by dividing the critical load at failure by the coated area.

2.2. Animal experimentation

Animal experimentation was carried out following the procedures conforming to the standards of the Institutions Animal Ethical Committee of the West Bengal University of Animal and Fishery Sciences, India. Eighteen clinically healthy adult New Zealand white rabbits (age 12–15 months) of either sex, weighing 2.5–3 kg, were used in this study. They were randomly distributed into three groups of six animals each: control (group I) i.e. uncoated pins with defects and no treatment, implanted with HAp coated pins (group II) and β-TCP coated pins (group III). After routine preoperative preparation, the rabbits were anaesthetized using combination of xylazine hydrochloride and ketamine hydrochloride anaesthesia as per the standard protocol described by Sedgwick [29]. The diaphysis of tibia was approached through routine surgical procedure. Prior to implantation of intramedullary implants, a rectangular defect of 10 mm length and 5 mm breadth was created by removing a piece of full thickness cortical bone by electrically operated micromotor-based dental drill and subsequently, the respective intramedullary pins were implanted within the medullary cavity of tibia of rabbits in normograde fashion using the standard method described by DeYoung and Probst [1] and Olmstead et al. [2]. The incisions were closed by suturing the muscle and subcutaneous tissues using chromic catgut (3/0). Skin was sutured with silk (3/0) in routine manner. The wound was covered with a protective dressing and bandages. Each animal was given injection cefotaxim sodium at a dose of 100 mg intramuscularly twice daily and paracetamol syrup once daily for 5 days. Routine dressing of the wound was done on 3rd, 5th and 7th postoperative days and skin sutures were removed on 10th postoperative day. Lameness, weight bearing/fracture repair capacity and associated signs of local inflammatory reactions were observed from the day of operation up to 60th day postoperatively and changes were evaluated by visual and manual examinations. Serum calcium [30], inorganic phosphorus [31] and alkaline phosphatase [32] were measured on day 0, 3, 7, 15, 30 and 60 postoperatively to assess the degree of inflammation and progress of bone healing. Anterio-posterior (A/P) radiographs were taken (300 mA medical diagnostic X-ray machine, M.E. X-Ray, India) immediately after implantation and subsequently on day 15, 30, 45 and 60 postoperatively of the operated limb. For histological investigation, bone samples were collected from both defect and normal area from the animals at day 60 postoperatively. The decalcified tissues were processed in a routine manner and 4 μm sections were cut with microtome and stained with hematoxylin and eosin to observe the matrix formation and conditions. Finally, fluorochrome was observed by injecting oxytetracycline dehydrate (Pfizer India, India) intramuscularly, at a dose rate 50 mg/kg body weight on days 48, 49 and later after 6 days interval on days 55 and 56 (2–6–2 manner) post-operatively for double toning of new bone. Undecalcified ground sections were prepared from the implanted segments of bone and were ground to 20 μm thickness using different grades of sand paper by rubbing under moderate pressure. Final grinding was done over the hone under moderate pressure using slow circular motions. The ground-undecalcified sections were observed under ultraviolet incidental light with an Orthoplan microscope (Excitation filter, BP-400 range; Leitz, USA) for tetracycline labelling to determine the amount and source of newly formed bone.

3. Results and discussions

3.1. In vitro structural characterizations

Phase and crystallographic features of coating obtained after MIPS technique both before and after heat treatments at 600 °C are given in Figs. 2 and 3 separately for HAp and β-TCP, respectively. Just for the purpose of comparison, the data for the as-synthesized powders, and powders/granules fired at 1250 °C (and 1200 °C) are incorporated in the respective Figs. 2 and 3. Crystalline phase of HAp phase was retained after plasma spraying and post heat treatment of this coating material (Fig. 2d). However, in case of β-TCP powder, the structure was decomposed after plasma spraying and post-heat treatment (Fig. 3d). New phases formed were α-TCP (JCPDS 09-0348) and calcium phosphide oxide (JCPDS 80-0410). In addition, the respective positions of the XRD peaks were well matched with JCPDS 74-0566 (calcium hydroxide phosphate or hydroxyapatite, Figs. 2a and 3a), 09-0432 (crystalline hydroxyapatite, Fig. 2b) and 09-0169 (pure β-tri calcium phosphate, Fig. 3b).

The degree of crystallinity for HAp granules, as sprayed and 600 °C heat-treated HAp coatings were ∼98%, 80% and 91%, respectively. Initial reduction in crystallinity of HAp granules was because of unmelted HAp particles in as-MIPS coating while the later enhancement reflects presence of more crystalline phase formation in the 600 °C heat-treated coating. Further increase of post heat-treatment temperature caused an adverse effect of substrate e.g. SS316L [33] and coating crystallinity [34] and hence, was not attempted in the present work. As-sprayed and 600 °C heat-treated β-TCP coating had ∼(58, 16.5 and 15.8%) and ∼(39.7, 15.5 and 10.4%) of β-TCP, α-TCP phase and Ca_4P_2O, respectively. This data revealed a reduction in phase content of the aforesaid phases in the heat treated β-TCP coating. A corresponding similar reduction was noted in crystallinity e.g. crystallinity of the as-sprayed and 600 °C heat treated β-TCP coating were ∼90.3 and 65.6%, respectively. Owing to its phase content as well as crystallinity, as-sprayed β-TCP coated intramedullary pins were finally selected for in vivo animal trial. Due to the same justifications, post heat-treated HAp coated pins were chosen.

FTIR data for as-sprayed MIPS coatings and coatings after heat treatment at 600 °C are given in Figs. 4 and 5 for HAp and β-TCP, respectively. In addition, the spectrums of powders/granules fired at 1250 °C (and 1200 °C) are incorporated for the purpose of comparison only. For the as sprayed HAp coating (Fig. 4b) the strong peaks at 1039 and 1092 cm^{-1} corresponded to stretching mode of PO_4^{3-} and those at 569 and 600 cm^{-1} related to bending modes of PO_4^{3-}. The peak at 877 cm^{-1} may be ascribed to a symmetric P–OH stretching vibration of HPO_4^{2-} groups. There exists a weak band at 962 cm^{-1} attributed to absorbed OH^-. The band at 3446 cm^{-1} might have come from lattice H_2O because this band exists in the range of 3550–3200 cm^{-1} for hydrated H_2O. Further, the additional peak at 3569 cm^{-1} band is assigned to the bulk OH^- ions in the fired compositions also. The FTIR spectra of HAp are consistent with those of reported by Ota et al. for pure HAp

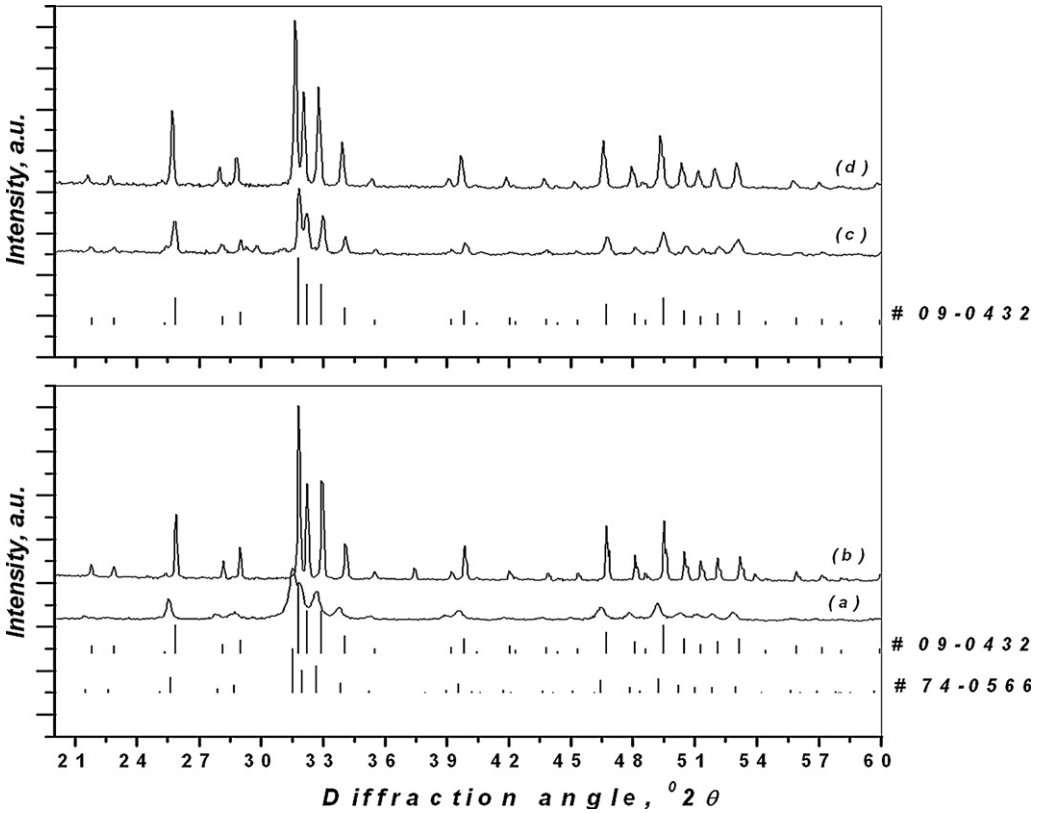

Fig. 2. XRD pattern of powders and coatings (for HAp): (a) as dried powder, (b) sintered (1250 °C) granule, (c) as sprayed coating and (d) heat treated (600 °C) coating.

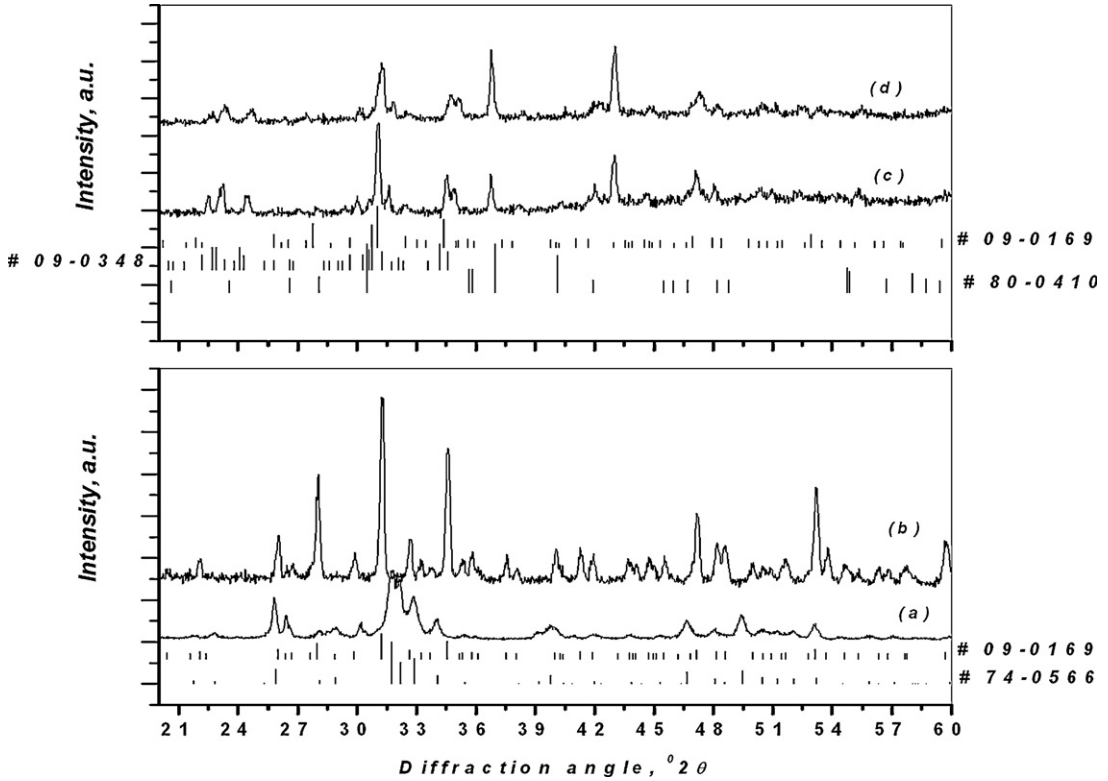

Fig. 3. XRD patterns of powders and coatings (for β-TCP): (a) as dried powder, (b) sintered (1200 °C) granule, (c) as sprayed coating and (d) heat treated (600 °C) coating.

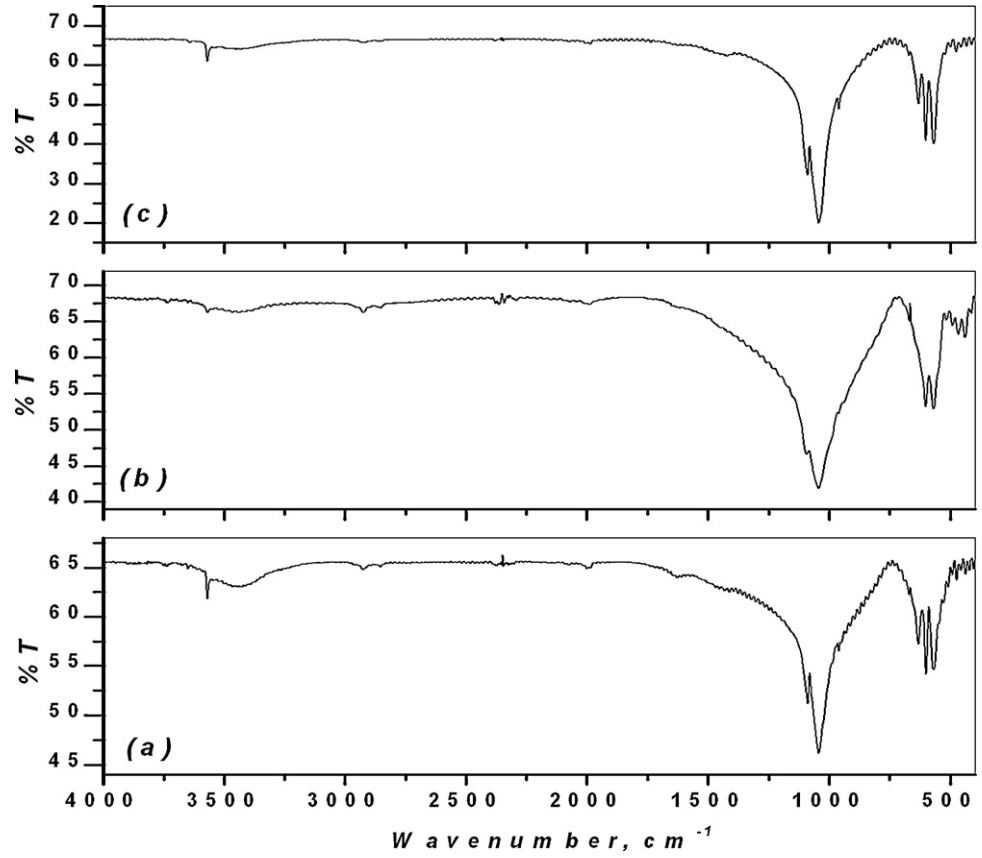

Fig. 4. FTIR spectrum of powders and coatings (for HAp): (a) sintered (1250 °C) granule, (b) as-sprayed coating and (c) heat treated (600 °C) coating.

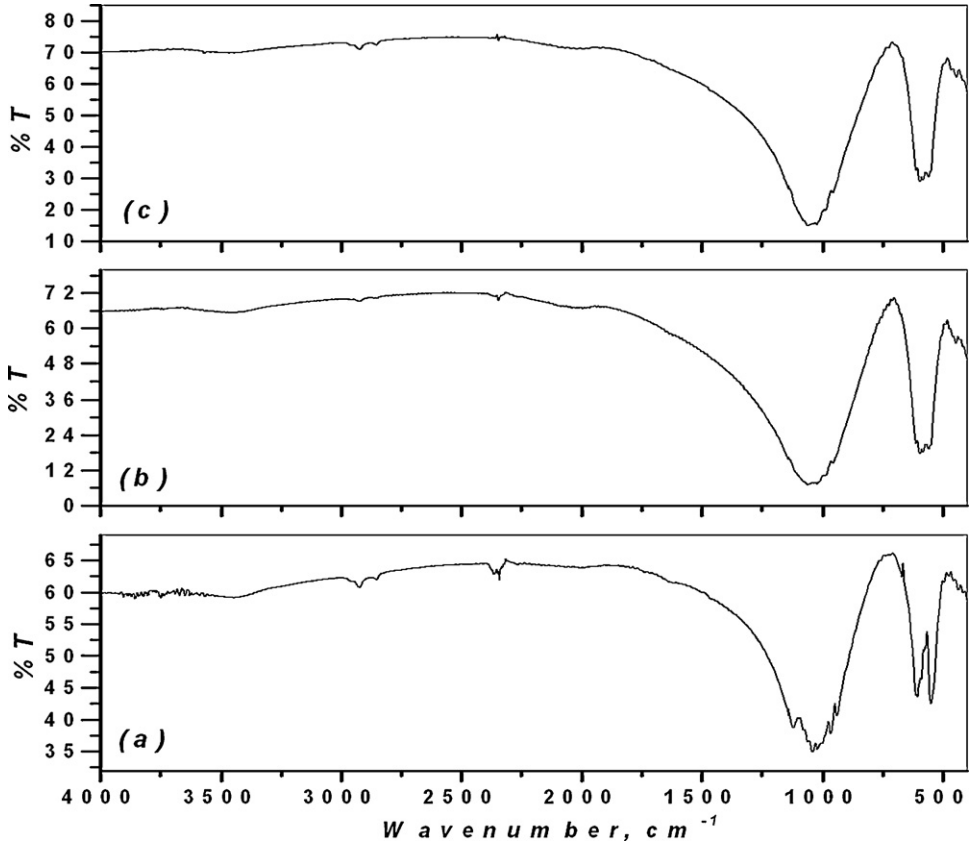

Fig. 5. FTIR spectrum of powders and coatings (for β-TCP): (a) sintered (1200 °C) granule, (b) as-sprayed coating and (c) heat treated (600 °C) coating.

powder [35]. The peak at 1092 cm^{-1} corresponding to PO_4^{3-} band had merged giving rise to a broad band indicating the presence of other Ca–P compounds and most likely, formation of some amorphous HAp. The decrease in transmittance at 3446 cm^{-1} (Fig. 4b) for the as-sprayed coating indicated that some of the hydroxyl groups (OH^-) were driven off during the high temperature process. This was due to dehydroxylation during spraying in which some MIPS-HAp might have been converted to oxyhydroxyapatite (OHAp) with the approximate formula $Ca_{10}(PO_4)_6(OH)_{2-2x}O_x\square_x$(□ = vacancy, $x < 1$) [34]. Post heat-treatment however gave the recovery of transmittance value at 3569 cm^{-1}.

In case of MIPS-TCP coating (Fig. 5), the range of 800–1200 cm^{-1} exhibited a wide transmission band typical of tetrahedral anions XO_4^n, in particular, PO_4^{3-}. The observed PO_4^{3-} transmission peaks around 1040–1122, 610 and 551 cm^{-1} are due to β-TCP [36]. The band at 1436.9 cm^{-1} is probably from carbonate, commonly found in both synthetic TCP and natural bone [37]. It has been found from Fig. 4b and c that one of the transmission bands for the phosphate (PO_4^{3-}) groups occurred at 1092 cm^{-1}. The larger bulge at the left side of the spectrum was indicative of the presence of some amorphous materials or moisture. On the other hand, data presented in Fig. 5b and c showed typical phosphate groups in the region 1100–950 cm^{-1} that were possibly hydrated too. But, no structural evidence for OH^- formation could be noticed. There were slight shift of the peaks around 1024, 611 and 559 cm^{-1} which may be due to the structural reorientation of the phosphate group from the parent pure β-TCP to the as-prayed and heat treated coating (Fig. 5b and c).

From both XRD (Figs. 2 and 3) and FTIR data (Figs. 4 and 5) it was found that the as-prepared powders were composed of calcium deficient hydroxyapatite, which when fired at their respective calcination temperature become poly-crystalline HAp or β-TCP depending on initial stoichiometry and based on the following reaction [38,39]:

$$Ca_{10-x}(HPO_4)_x(PO_4)_{6-x}(OH)_{2-x} \rightarrow$$

$$(1 - x)Ca_{10}(PO_4)_6(OH)_2 + 3x\beta - Ca_3(PO_4)_2 + xH_2O$$

where x is the calcium deficiency.

Typical SEM image of heat-treated MIPS-HAp coating is shown in Fig. 6a and b. The microstructure of the coating was heterogeneous and highly porous. The average volume percent open porosity was ∼20% as measured by the image analysis technique applied to SEM photomicrographs. Splat size was ∼50–70 μm, macropore size was ∼10–30 μm and micropore size was ∼1 μm. Intra and inter-splat microcracks were distributed all over the as sprayed MIPS coating (Fig. 6a) along with unmelted HAp particles. The pores were formed because of poor bonding between adjacent splats and microcracking arose from shrinkage of the splat during quenching and subsequent differential thermal contraction between substrate and coating. Post heat-treated MIPS HAp coating microstructure (Fig. 6b) appeared as if it were more densified on a comparative scale (ca. Fig. 6a).

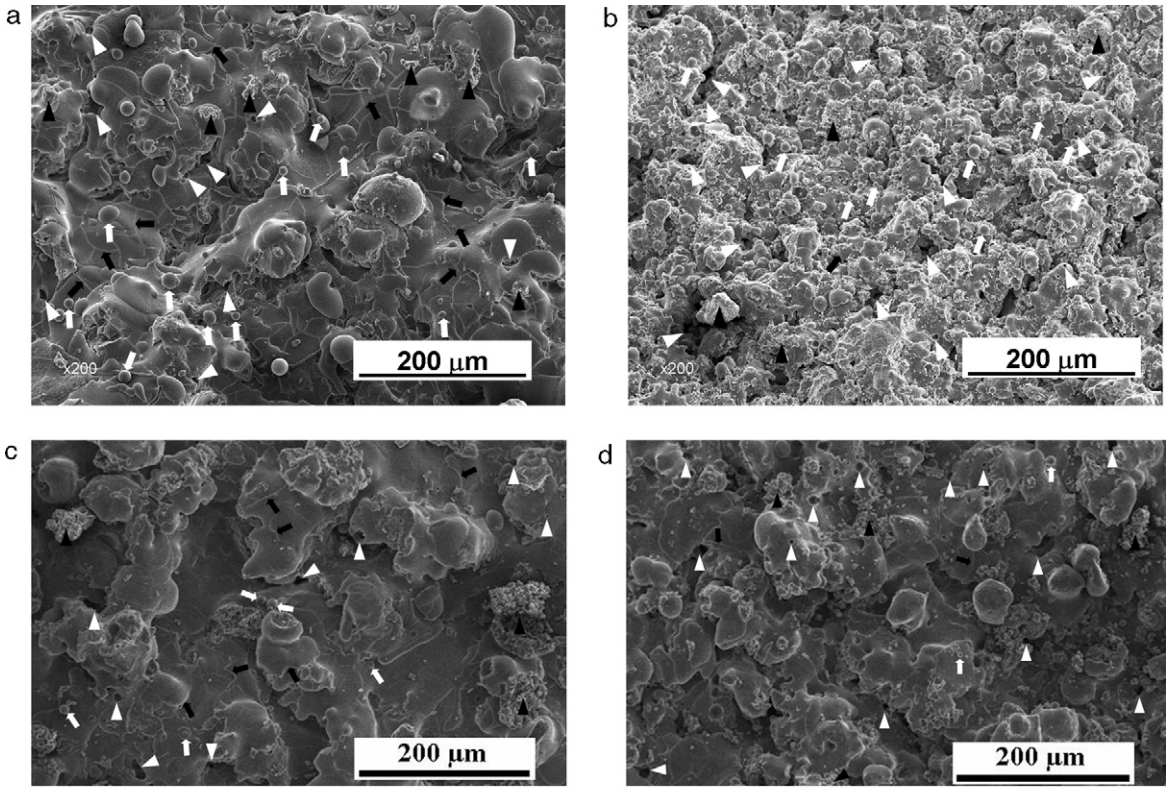

Fig. 6. SEM photomicrograph of plasma spray coating for HAp and β-TCP; (a) HAp as sprayed: pores (white bold arrow heads), unmelted splats retaining a non-flattened core (white bold arrow), deformed splats (black bold arrow heads), splat cracks (black bold arrow), (b) HAp after post heat treatment: pores (white bold arrow heads), unmelted splats retaining a non-flattened core (white bold arrow), deformed splats (black bold arrow heads), splat cracks (black bold arrow), (c) β-TCP as sprayed: pores (white bold arrow heads), unmelted splats retaining a non-flattened core (white bold arrow), deformed splats (black bold arrow heads), splat cracks (black bold arrow) and (d) β-TCP after post heat treatment: pores (white bold arrow heads), unmelted splats retaining a non-flattened core (white bold arrow), deformed splats (black bold arrow heads), splat cracks (black bold arrow).

In case of MIPS-TCP coating almost same observation could be noticed as that of HAp (Fig. 6c and d). Only difference being that the coating cracks were less predominant than the corresponding HAp coating, possibly due to less crystallinity of β-TCP crystals when exposed to plasma temperature. Further, lesser frequency of unmelted particles was noticed. Pores usually fell in the size range of ∼1 μm. After heat treatment (Fig. 6d), it appeared as if the MIPS-TCP coating microstructure became more homogeneous with lesser amount of unmelted particles, inter and intra-splat cracks as well as micropores. More amorphous content in the β-TCP coating (Fig. 3) also possibly helped for healing up of the microcracks when heat-treated. At same spraying powers, the HAp particles were poorly melted. When they impacted on the substrate (or the already formed coating), they were not able to spread out completely to form splats and therefore, could not conform to the surface [20,40]. However, in case of β-TCP, the condition actually reversed owing to its lower crystallinity and spread nicely when impacted. Typical HAp/β-TCP coating thickness on the substrate was found to be 150–200 μm.

The measured bonding strength for HAp and β-TCP coating was found to be ∼13 MPa and 11.6 MPa, respectively. These values were quite comparable with the reported corresponding values (∼2–30 MPa) for the macro-plasma deposited coating [41,42]. Owing to its higher crystallinity, phase purity, lesser coating cracks, high adhesion strength and moderate-to-high amount and distribution of micropores, MIPS coated and heat treated HAp substrates were selected for further in vivo studies and due to same justification MIPS coated and as-sprayed (non heat-treated) β-TCP substrates were selected for further animal trials.

3.2. In vivo characterizations

3.2.1. Local inflammatory reactions and healing of wound

Only a mild swelling was observed at the operative site, which reached maximum on the 6th postoperative day and thereafter, it subsided gradually and returned to normalcy within 10 postoperative days. All the animals of three groups showed signs of lameness in the immediate postoperative period without showing any visible difference between different groups. Weight bearing capacity in each animal subject gradually improved as signs of inflammation subsided.

The lameness and a transient inflammatory response were observed in the immediate postoperative period may be associated with the surgical trauma. Subsequently, lameness disappeared gradually, which suggest that inflammation was subsided and fracture was getting stable. This finding was in

agreement with the observations of ulnar fracture in dog by Shukla [43] and in rabbit by Singh [44]. In the present study no foreign body response or toxicity was elicited and hence all the implants were accepted without any undesirable effect.

Clinical signs were of little importance in evaluating the process of healing after reconstruction of bone defects by different types of intramedullary implants. However, type of wound healing and restoration of function provided an idea about the status of soft tissue formation and bone healing thereby. All the surgically created defect areas and the implants were well placed, well accepted and tolerated by the animals, causing no serious inflammation in the surrounding tissue. Healing was uneventful in all animals and there was no evidence of rejection of implant in any case. The clinical features of the present study corroborated with the findings of Holmes et al. [45].

3.2.2. Serum biochemical observation

The present study showed highly significant changes in serum alkaline phosphatase activity (IU/L) at different time of fracture healing in all three experimental groups of animal estimated on six different time intervals (Fig. 7a). The ALP values started to increase in all groups of animals post-operatively reaching to its peak at 15th day postoperatively. On 60th day postoperatively, it started to reach normal level. The findings of serum calcium estimation showed no significant changes in serum calcium level (mg/dl) through out the study period (Fig. 7b). In group I, II and III, serum calcium values were 9.71 ± 0.08, 10.34 ± 0.22 and 10.67 ± 0.16 respectively on '0' day, which did not alter remarkably at time of observation in any groups. The serum phosphorus level (mg/dl) also showed no statistically significant changes like serum calcium values during the different stages of fracture healing in

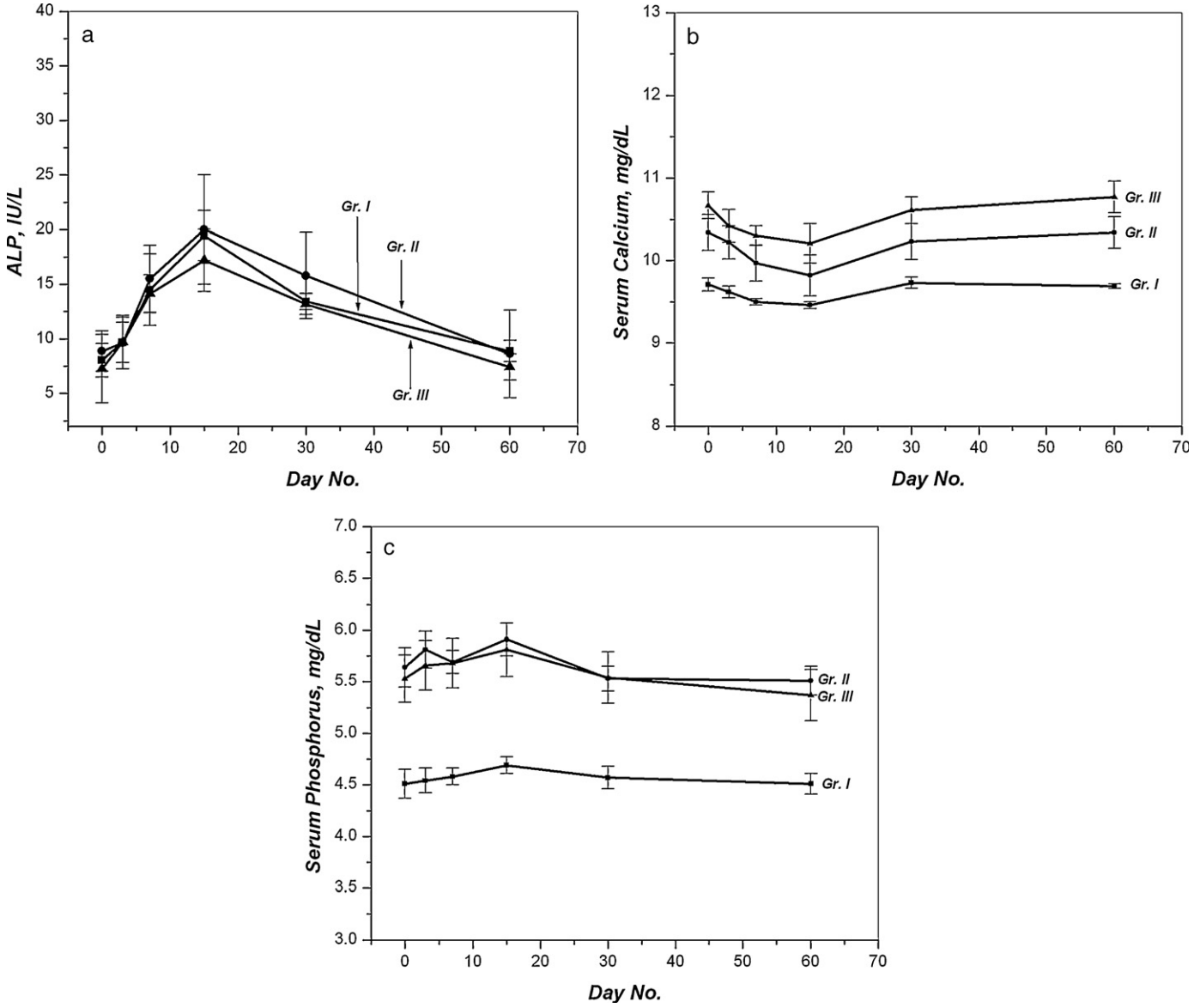

Fig. 7. Changes in serum (a) alkaline phosphatase activity (IU/L), (b) calcium estimation (mg/dl) and (c) phosphorous level (mg/dl) at different time of fracture healing (for group I, II and III animals) with $n = 6$.

all the groups (Fig. 7c) except a non-significant rise to its peak: 4.69 ± 0.08, 5.91 ± 0.16 and 5.81 ± 0.26 in group I, II and III respectively on 15th postoperative day. These were gradually reduced however and returned back to normal level within 60 day postoperatively.

There was highly significant elevation in serum ALP level in all the groups up to 15th postoperative day and thereafter, the values returned to normal within 60th postoperative day. Similar result was reported by Saraswathy et al. [46].

Alkaline phosphatase works best at alkaline pH, and thus the enzyme itself is inactive in the blood. Alkaline phosphatase acts by splitting off phosphorus (an acidic mineral) creating an alkaline pH. The osteoblast heals through osteogenesis [47] after secreting alkaline phosphatase enzyme [48]. The rising level of serum ALP in different groups from base values was different, suggesting the different rate of osteogenesis as per quantitative and qualitative activity of osteoprogenitor cells. Thus, enhanced activity of osteoblast leads to increased ALP activity up to 15th postoperative day, which came to normal afterward gradually, when callus formation ceased [49].

In the present study, serum calcium level showed no significant changes at any intervals of the study period. Similar results were reported by Speed [50] and Pandey and Udupa [51], who opined for non-correlation between fracture healing and serum calcium level. However, an increased serum calcium levels after fracture were reported by Suryawanshi et al. [52]. There was a non-significant reduction in serum calcium values up to 15th post-operative day in all the animals. Such decrease in the level of serum calcium could be due to increased urinary excretion after traumatic bone injury [46].

Serum phosphorus level exhibited a non-significant increase up to 15th postoperative day which gradually reduced and returned back to normal in 60th day postoperatively. Increase in serum phosphorus level during early stages of fracture healing [46,50,51] is also reported in few literatures. The increase in serum phosphorus concentration might be attributed to the enhanced mineralization during this period. Moreover, necrotic disintegration of the cells at the fracture site was responsible for early rise in phosphorous levels [46]. However, the difference in serum phosphorus levels during different stages of bone healing was not significant.

The HAp coatings provide ‘‘bone bonding’’, promote osseointegration and minimize adverse reaction by provision of a biocompatible phase. Further, with increasing thickness of the coating (150–160 μm), concentration of metal ions released to the body decreased [53].

3.2.3. Radiographic evaluation

Fig. 8a–c shows the radiographic observation of different groups (group I, II and III, respectively) taken on 15th, 30th, 45th and 60th post-operative days. The results are analyzed and summarized schematically in Table 3. The observations were divided according to the following radio-density classifications: ‘+’ was indicative of mild/present, ‘++’ of moderate, ‘+++’ of significant and ‘−’ was of absent. In Fig. 8a, day ‘0’ showed radio-lucent rectangular cortical defect on proximal third of the tibia. The pin margin was uniformly dense and had distinct details. On day ‘15’, periosteal reaction around the cortical defect was evident. On day ‘30’, bone defect was obliterated by newly formed osseous tissue with evidenced cortical continuity in the defect area. On day ‘45’, osseous tissue was present in the defect but still the bony defect was evident on radiograph. Finally, on day ‘60’, bony defect was not visible on radiograph and the newly formed osseous tissue was more organized and compacted. In hydroxyapatite coated group (Fig. 8b), radiograph taken on day ‘0’ showed radio-lucent rectangular cortical defect on proximal third of the tibia. Intramedullary pin was present beyond the bone defect area up to the mid shaft of the bone and the pin margin was indistinct. On day ‘15’, the defect area showed indistinct margins and reduced density. On day ‘30’, bone defect was obliterated by newly formed osseous tissue with evidence of cortical continuity in the defect area. A central radio-lucent area in the defect area was still visible. On day ‘45’, osseous tissue obliterated the defect leaving only a central radio-lucent area and a cortical continuity. On day ‘60’, bone defect was obliterated by newly formed osseous tissue with established cortical continuity in the defect area. No bony resorption around the pin was evidenced. In case of β-TCP coating (Fig. 8c), radiograph on day ‘0’ was identical with the other two cases. On day ‘15’, the defect area showed indistinct margins and reduced density. On day ‘30’, bone defect was obliterated by newly formed osseous tissue with established cortical continuity in the defect area. On day ‘45’, bony defect was not visible on radiograph and there was evidence of formation of bridging callus. On day ‘60’, finally, bone defect was obliterated by newly formed osseous tissue with established cortical continuity in the defect area.

Critical evaluation of radiographs taken at different intervals in animals of group I revealed no significant evidence of fracture union as compared to other two groups. However, at the initial stage, minimal periosteal reaction and smoothing edges of cortical bone defects were noticed. This may be due to the fact that the bone surfaces were in direct contact with metallic implant that might have caused ‘‘metallosis’’ [54]. Subsequently, there was substantial reduction of gap size by newly formed osseous tissue, making the defect more round and smooth. Similar finding was also reported by Bolander and Balian [55].

3.2.4. Histological observations

In uncoated group, section showed cancellous bone and well developed marrow spaces. Bone lamella was lined by osteoblasts. Marrow cavity contained adipose tissue with marrow material (Fig. 9a). On the other hand, hydroxyapatite coated group showed complete ossification with developed Havarsian canals and well-defined peripherally placed osteoblasts. Blood vessels in Havarsian spaces were found to be well-developed with very little marrow amount at spaces. Few particles of non-absorbed biodegradable material were seen in the lamellar cortical bone and in marrow space as refractile crystalloid structure (Fig. 9b). In β-TCP coated group, section showed moderately differentiated lamellar bone in the cortical part containing a few granular foreign body materials. Peripheral part of the cortex showed presence of woven bone

Fig. 8. Radiographic observation at fracture site, taken after '0', '15', '30', '45' and '60th' day postoperatively for (a) group I, (b) group II and (c) group III animals.

and marrow space showed evidence of angiogenesis with focal development of marrow material in the midst of unabsorbed foreign granular debris (Fig. 9c). Histologically, it is revealed that bone formation in defect area was more in β-TCP coated group as compared to HAp coated and uncoated group based on woven bone formation and angiogenesis.

Histological observations provided detailed information about the cellular events during incorporation of different types of ceramic-coated implants. In group I animals, histological section showed formation of cancellous bone with well-developed marrow spaces. Bone lamella was lined by osteoblasts. However, complete ossification with developed Havarsian canals and well-defined peripherally placed osteoblasts were not observed as compared to group II and III animals. This might be due to the fact that the inert metallic materials (i.e. intramedullary pin pin) do not form a chemical bond with tissues, but rather a fibrous tissue capsule is formed. This observation supported the findings of Nguyen et al. [56]. In group II and III animals, there were complete ossification with developed Havarsian canals and well-defined peripherally placed osteoblasts. This might be due to direct chemical implant-bone contact, thus reducing the time required for osseointegration. In order for a material to chemically attach to bone, spontaneous formation of bone-mineral like calcium phosphate (Ca–P) on the materials surface in physiological environments is needed [57]. Calcium phosphate coatings are required as a means of improving ''bone bonding'' and promoting more rapid osseointegration [58,59].

Table 3
Radiographic features at different days of interval in different groups.

Group	Uncoated group	HAp coated group	β-TCP coated group
Periosteal reaction – '15' day	+	+	++
Periosteal reaction – '30' day	+	+	+
Periosteal reaction – '45' day	++	+	–
Periosteal reaction – '60' day	+	–	–
Radiodensity of the defect area 30 days	+	+	++
Radiodensity of the defect area 45 days	+	++	++
Radiodensity of the defect area 60 days	++	+++	+++
Visible bone defect 45 days	+	+	–
Visible bone defect 60 days	–	–	–
Resorptive changes 30 days	+	+	+
Resorptive changes 45 days	+	+	–
Resorptive changes 60 days	+	–	–
Cortical continuity 45 days	–	–	+

+ mild/present; ++ moderate; +++ marked; – absent.

The mechanisms of the bonding of bioactive ceramics with bone have been documented for bioactive glass, glass-ceramics, HAp and other calcium phosphate materials [60,61]. A calcium phosphate-rich layer formed at the implant-bone interface is evidence of chemical bonding for the surface-active materials. For permanent implants, it is essential that the surrounding bony tissue integrates well (osseointegration) and the surface of the implant favours the process of cell attachment, adhesion, proliferation and tissue growth [60] leading to stable implant anchorage [61–64]. Whenever an implant is brought in contact with bone, blood proteins are adsorbed onto the surface of the implant. Though other proteins attach first, eventually mostly fibrin is found, which contacts both the bone and implant [65]. Along these fibrin fibres, osteogenic cells from the marrow and the endosteum, migrate towards the implant and during this migration differentiate into mature osteoblasts.

3.2.5. Fluorochrome labelling study

In uncoated group, when viewed under ultraviolet incident light, the ultraviolet light imparted golden yellow fluorescence as tetracycline marked the new bone. This golden yellow fluorescence was present as a narrow area in the defect site whereas, host bone appeared dark homogenous sea green colour. The defect was completely filled with newly formed cancellous bone and appeared as homogenous non-fluorescent area (Fig. 10a). Union in the defect site of bone was more-or-less complete in most of the animals. In hydroxyapatite coated group, under fluorescent microscope, the defect was visualized as a line of golden yellow fluorescence whereas, the host bone appeared as homogenous dark sea green colour. In this group, the activity of new bone formation was marked. Within this new osteoid tissue, which completely filled the bone defect, crossing over of new bone trabeculae was evident. Few resorption

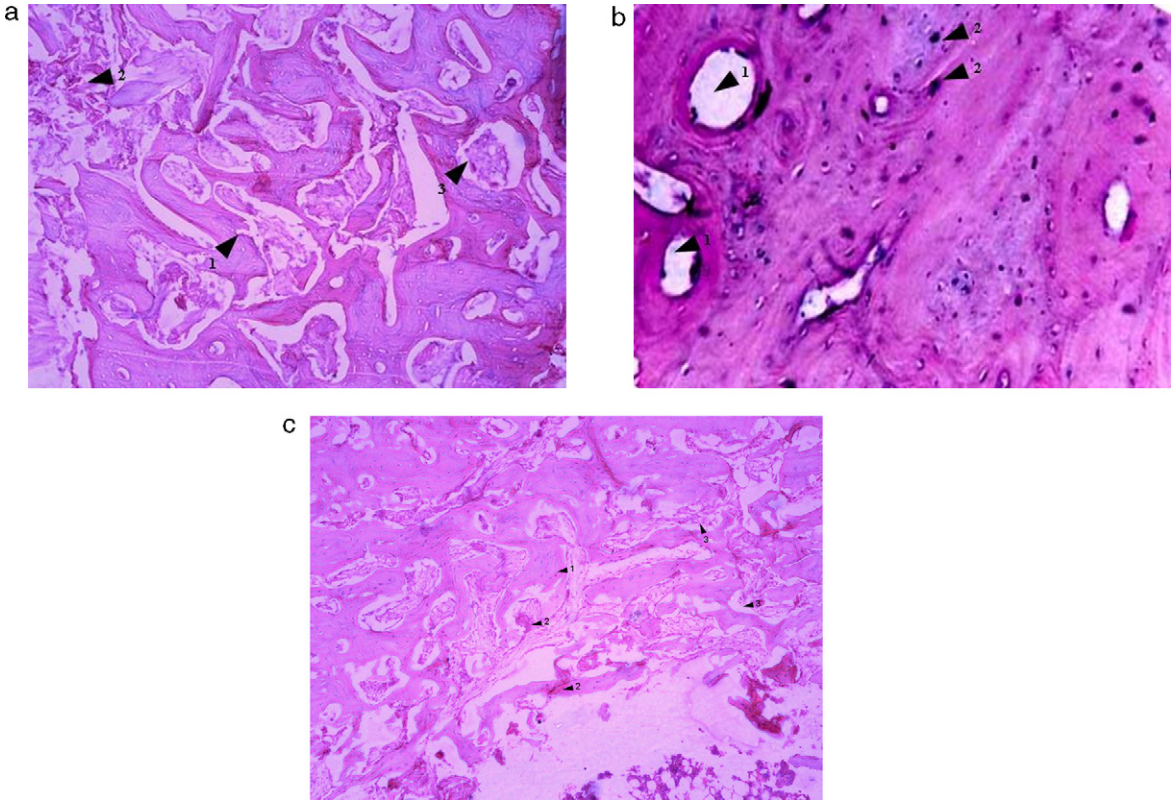

Fig. 9. Histopathology: photomicrograph of (a) group I animal showing cancellous bone (1) and well-developed marrow spaces. Bone lamella (2) is lined by osteoblasts. Marrow cavity contained adipose tissue (3) with marrow material; (b) group II animal had complete ossification with developed Havarsian canals (1), well-defined peripherally placed osteoblasts (2) and angiogenesis; (c) group III animal had well-differentiated lamellar system (1) with moderate osteoblastic activity, translucent material (2) deposited around perilamellar spaces and showing regenerative osteoclastic (3) activity. All micrographs were taken as HE ×10 magnification.

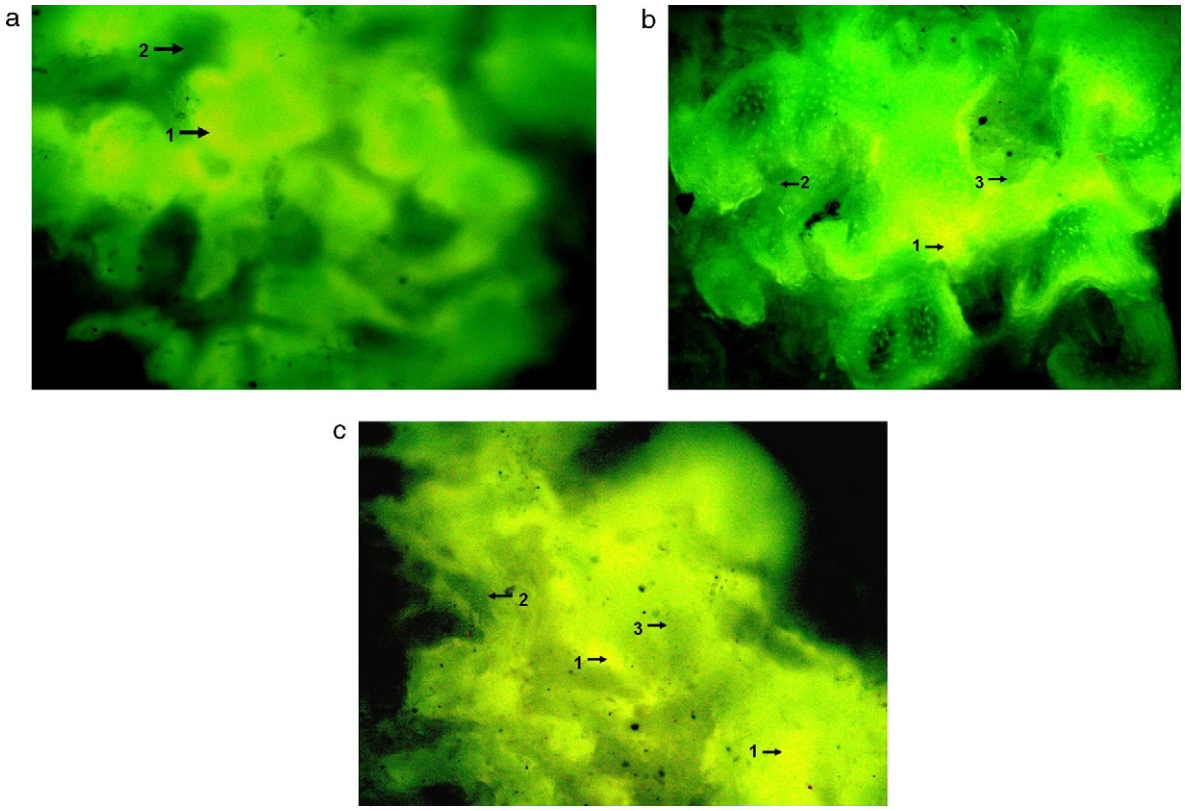

Fig. 10. Fluorochrome labelling study: photomicrograph showing (a) golden yellow fluorescence (1) as a narrow area in the defect site and old bone with sea green appearance (2) in group I animal, (b) line of golden yellow fluorescence (1) with moderate activity of new bone formation in group II animal and (c) old bone representing sea green appearance and (3) resorption cavities in group III animal. Fluorochrome labelling study: photomicrograph showing double tone golden yellow fluorescence (1) in wider zone in the defect site in group III animal. (2) Old bone representing sea green appearance and (3) resorption cavities.

cavities were also present (Fig. 10b). In β-TCP coated group, microphotograph viewed under fluorescent light (6.3 × 10 magnification) imparted a double tone golden yellow fluorescence in wider zone in the defect site and the host bone evinced homogenous dark sea green colour. However, at some places, the host bone showed newly formed woven bone, which was cancellous in nature. Further, in the defect area, some light sea green homogenous colour appeared amongst the trabeculae suggesting newly formed bony tissue became matured. At places, few resorption cavities were also present (Fig. 10c).

Several methods exist to examine newly formed bone using specific bone markers and labelling techniques [66,67]. The tetracycline labelling method was introduced to measure the quantity of newly formed bone as tetracycline molecule is having fluorescence property in ultraviolet light. Oxytetracycline follows the ionized calcium and the fixation by a process of adsorption, which is restricted to areas where active deposition of mineralized tissue is taking place [68]. The labelled new bone and old bone emitted bright golden yellow and dark sea green fluorescence, respectively. These parts provide immense value in studying gross bone architecture and histological mapping of new bone formation using fluorescent bone markers. In the present study, oxytetracycline at a dose of 50 mg/kg body weight (2–6–2 pattern) before end of study was proved to be sufficient to quantify the extent of new bone formation. In animals of group I, most of the bone defects were occupied by homogenous nonfluorescent area suggesting little amount of new bone formation but the process of new bone formation was active from both the ends which corroborated the findings of Singh [44] and Nandi et al. [69,70]. However, the golden yellow fluorescence in a narrow area was also observed in the present study suggesting new bone formation in the defect site. Thus, oxytetracycline labelling study demonstrated that HAp and β-TCP coated intramedullary pins contributed to new bone formation in the defect area by host bone which is similar with the observations of Singh [44] and Nandi et al. [69,70]. Resorption cavities were present more in β-TCP coated group as compared to HAp coated group suggesting that the resorption and replacement of the bone was well under progress. Besides, the resorption cavities were indicative of initiation of bone remodeling [69,70].

Recently, Junker et al. [22] showed femoral condyle bone fixation using titanium alloy implant coated with a MIPS calcium phosphate compound in goat model. This pioneering work indeed indicated that the MIPS coated implant's performance was at least as good as that of a conventional macro-plasma HAp coated implant. This work emphasized the success of MIPS based implant on the basis of only histopathological study in vivo. They had starting material which had a comparatively lower crystallinity (e.g. 65% for MAPS coating, 67% and 80% for two types of MIPS coating, and reported a reduction of coating thickness due to the

dissolution of the amorphous phase between the remaining crystalline coating particles of HAp and presence of other calcium phosphate phase/s in the coating composition. The main focus of Junker et al. [22] was on the evaluation of mechanical stability of the MIPS coated implants. However, the main focus of the present work was to establish MIPS coating with highly crystalline pure HAP and β-TCP for bone fracture fixation application in terms of biocompatibility, functional stability, as well as osteoconductivity. Thus, the present work attempted a systematic study of HAp and β-TCP powder and their MIPS coating on SS316L intermedullar pin through extensive XRD, FTIR encompassing phase and chemical structure analysis, SEM studies elucidating microstructure evolution and finally application of MIPS coated actual implants in animal study on New Zealand white rabbits in terms of detailed blood bio-chemistry, histology, fluorochrome labelling and radiology based evaluation of suitability or otherwise. To the best of our knowledge prior to the present work there has not been any reported studies on success of MIPS coated β-TCP intermedullar pin implants for New Zealand white rabbits. The results have shown that the MIPS coated pure HAp and β-TCP intramedullary SS316L pins have better healing capabilities than uncoated intramedullary SS pins. Further, the MIPS coated intermedullary SS316L pins with β-TCP ceramics were found to have better bone formation and apposition compared to those of the MIPS HAp coated intermedullary SS316L pins. These promising results would strongly suggest to go for further extensive trials with animals, particularly with the MIPS-TCP coated implants, and if found suitable in terms of detailed blood bio-chemistry, histology, fluorochrome labelling and radiology based evaluation as well as mechanical stability, the same could be selected as a futuristic promising new biomaterial for human bone fracture fixation device. It is needless to say that the selection of HAp or β-TCP as material for MIPS coating on the given implant would also have to be decided by the quality of bone that needs to undergo fracture fixation.

4. Conclusions

A comparative study of the healing kinetics of surgically created artificial defects in the tibia of New Zealand white breed of rabbit using MIPS coated pure HAp and β-TCP was carried out. After optimizing the coating parameters w.r.t. thorough XRD, FTIR, SEM morphology analysis, suitable implants were used in vivo. Results of the biochemical, histological, radiographic and fluorochrome labelling revealed probably for the first time that the MIPS coated pure HAp and β-TCP intramedullary SS316L pins have better healing capabilities than uncoated intramedullary SS pins. Further, the MIPS coated intermedullary SS316L pins with β-TCP ceramics were found to have better bone formation and apposition compared to those of the MIPS HAp coated intermedullary SS316L pins. The bone defect healing was comparatively better due to ‘‘bone bonding’’ and osseointegration in β-TCP coated pin followed by the HAp coated and uncoated pins. The results of the present work established the superiority of MIPS HAp and β-TCP coated intramedullary SS316L pins over the uncoated conventional SS316L pins in fracture repair of surgically created artificial defects in the tibia of the rabbits.

Acknowledgements

The authors wish to express their sincere thanks to Professor Indranil Manna, Director, Central Glass and Ceramic Research Institute, Kolkata and the Dean, Faculty of Veterinary and Animal Sciences, West Bengal University of Animal and Fishery Sciences, Kolkata, India for their kind permission to use the facilities for the experimentation. The authors also express their gratitude to the Department of Science and Technology, New Delhi for Financial Support. Author A.D. also acknowledges the fellowships awarded by Council of Scientific and Industrial Research, New Delhi.

References

[1] D.J. DeYoung, C.W. Probst, Methods of internal fracture fixation-general principles, in: D.H. Slatter (Ed.), Textbook of Small Animal Surger, WB Saunders, Philadelphia, 1993, pp. 1610–1631.
[2] M.L. Olmstead, E.L. Egger, L.J. Wallace, A.L. Johnson, Principles of fracture repair, in: M.L. Olmstead (Ed.), Small Animal Orthopedics, Mosby, St. Louis, 1995, pp. 111–159.
[3] K.A. Thomas, J.F. Kay, S.D. Cook, M. Jarcho, The effect of surface macrotexture and hydroxylapatite coating on the mechanical strengths and histologic profiles of titanium implant materials, Journal of Biomedical Materials Research 21 (1987) 1395.
[4] M. Filiaggi, R.M. Pilliar, N.A. Coombs, Characterization of the interface in the plasma-sprayed HA coating/Ti-6AI-4V implant system, Journal of Biomedical Materials Research 25 (1991) 1211.
[5] D.P. Rivero, J. Fox, A.K. Skipor, R.N. Urban, J.O. Galante, Calcium phosphate-coated porous titanium implants for enhanced skeletal fixation, Journal of Biomedical Materials Research 22 (1988) 191.
[6] P. Ducheyne, Q. Qiu, Bioactive ceramics: the effect of surface reactivity on bone formation and bone cell function, Biomaterials 20 (23–24) (1999) 2287–2303.
[7] M. Rokkum, A. Reigstad, C.B. Johansson, T. Albrektsson, Tissue reactions adjacent to well-fixed hydroxyapatite-coated acetabular cups. Histopathology of ten specimens retrieved at reoperation after 0.3 to 5.8 years, The Journal of Bone and Joint Surgery 85 (3) (2003) 440–447.
[8] L. Zhao, K. Bobzin, F. Ernst, J. Zwick, E. Lugscheider, Study on the influence of plasma spray processes and spray parameters on the structure and crystallinity of hydroxylapatite coatings, Materialwissenschaft Und Werkstofftechnik 37 (6) (2006) 516–520.
[9] E. Lugscheider, K. Bobzin, L. Zhao, J. Zwick, Assessment of the microplasma spraying process for coating application, Advances in Engineering Materials 8 (7) (2006) 635–639.
[10] C.J. Li, B. Sun, Microstructure and property of Al_2O_3 coating microplasma-sprayed using a novel hollow cathode torch, Materials Letters 58 (1–2) (2004) 179–183.
[11] A. Dey, A.K. Mukhopadhyay, S. Gangadharan, M.K. Sinha, D. Basu, N.R. Bandyopadhyay, Nanoindentation study of microplasma sprayed hydroxyapatite coating, Ceramics International 35 (6) (2009) 2295–2304.
[12] C.J. Li, B. Sun, Microstructure and property of micro-plasma sprayed Cu coating, Materials Science and Engineering A 379 (1–2) (2004) 92–101.
[13] Y. Gao, X. Xu, Z. Yan, G. Xin, High hardness alumina coatings prepared by low power plasma spraying, Surface and Coatings Technology 154 (2–3) (2002) 189–193.
[14] R.S. Lima, K.A. Khor, H. Li, P. Cheang, B.R. Marple, HVOF spraying of nanostructured hydroxyapatite for biomedical applications, Materials Science and Engineering A 396 (1–2) (2005) 181–187.

[15] K.A. Gross, C.C. Berndt, H. Herman, Amorphous phase formation in plasma-sprayed hydroxyapatite coatings, Journal of Biomedical Materials Research 39 (3) (1998) 407–414.
[16] W. Tong, J. Chen, X. Li, Y. Cao, Z. Yang, J. Feng, X. Zhang, Effect of particle size on molten states of starting powder and degradation of the relevant plasma-sprayed hydroxyapatite coatings, Biomaterials 17 (15) (1996) 1507–1513.
[17] A. Dey, A.K. Mukhopadhyay, S. Gangadharan, M.K. Sinha, D. Basu, Characterization of microplasma sprayed hydroxyapatite coating, Journal of Thermal Spray Technology 18 (4) (2009) 578–592.
[18] C.E. Mancini, C.C. Berndt, L. Sun, A. Kucuk, Porosity determinations in thermally sprayed hydroxyapatite coatings, Journal of Materials Science 36 (16) (2001) 3891–3896.
[19] H. Dingyong, Z. Qiuying, Z. Lidong, S. Xufeng, Influence of microplasma spray parameters on the microstructure and crystallinity of hydroxyapatite coatings, Chinese Journal of Materials Research 21 (6) (2007) 659–663.
[20] A. Dey, A.K. Mukhopadhyay, S. Gangadharan, M.K. Sinha, D. Basu, Development of hydroxyapatite coating by microplasma spraying, Materials and Manufacturing Processes 24 (12) (2009) 1321–1330.
[21] T.M. Lee, B.C. Wang, Y.C. Yang, E. Chang, C.Y. Yang, Comparison of plasma-sprayed hydroxyapatite coatings and hydroxyapatite/tricalcium phosphate composite coatings: in vivo study, Journal of Biomedical Materials Research 55 (3) (2001) 360–367.
[22] R. Junker, P.J.D. Manders, J.G. Wolke, Y. Borisov, J.A. Jansen, Bone-supportive behavior of microplasma-sprayed CaP coated implants: mechanical and histological outcome in the goat, Clinical Oral Implants Research 21 (2) (2010) 189–200.
[23] B. Kundu, M.K. Sinha, M.K. Mitra, D. Basu, Fabrication and characterization of porous hydroxyapatite ocular implant followed by an in vivo study in dogs, Bulletin of Materials Science 27 (2) (2004) 133–140.
[24] B. Kundu, A. Lemos, C. Soundrapandian, P.S. Sen, S. Datta, J.M.F. Ferreira, D. Basu, Development of porous hydroxyapatite and β-tri calcium phosphate scaffolds by starch consolidation with foaming method and drug-chitosan bilayered scaffold based delivery system, Journal of Materials Science: Materials in Medicine (2010), doi:10.1007/s10856-010-4127-0.
[25] ASTM Standard B212-09, Standard test method for apparent density of free-flowing metal powders using the Hall flowmeter funnel, in: American Society for Testing, Materials: Metallic, Inorganic Coatings, Metal Powders, Metal Powder Products, vol. 02.05, ASTM International, West Conshohocken, PA, 1999.
[26] H.P. Klug, L.E. Alexander, X-Ray Diffraction Procedures: for Polycrystalline and Amorphous Materials, 2nd ed., Wiley-VCH, New Jersey, 1974
[27] E. Landi, A. Tampieri, G. Celotti, S. Sprio, Densification behaviour and mechanisms of synthetic hydroxyapatites, Journal of the European Ceramic Society 20 (14–15) (2000) 2377–2387.
[28] ASTM Standard C633-01, Standard test method for adhesion or cohesion strength of thermal spray coatings, in: American Society for Testing and Materials: Metallic and Inorganic Coatings; Metal Powders and Metal Powder Products, vol. 02.05, ASTM International, West Conshohocken, PA, 2001.
[29] C.J. Sedgwick, Anesthesia for rabbits, The Veterinary Clinics of North America 2 (3) (1986) 731–736.
[30] P. Trinder, Colorimetric micro-determination of calcium in serum, Analyst 85 (1017) (1960) 889–894.
[31] G. Gomori, A modification of the colorimetric phosphorous determination for use with the photoelectric colorimeter, Journal of Laboratory and Clinical Medicine 27 (1942) 955–976.
[32] P.R. Kind, E.J. King, Estimation of plasma phosphatase by determination of hydrolysed phenol with amino-antipyrine, Journal of Clinical Pathology 7 (4) (1954) 322–326.
[33] T.M. Sridhar, U. Kamachi Mudali, M. Subbaiyan, Sintering atmosphere and temperature effects on hydroxyapatite coated type 316L stainless steel, Corrosion Science 45 (10) (2003) 2337–2359.
[34] C.C. Chen, S.J. Ding, Effect of heat treatment on characteristics of plasma sprayed hydroxyapatite coatings, Materials Transactions 47 (3) (2006) 935–940.
[35] Y. Ota, T. Iwashita, T. Kasuga, Y. Abe, Novel preparation method of hydroxyapatite fibers, Journal of the American Ceramic Society 81 (6) (1998) 1665–1668.
[36] R.Z. LeGeros, Calcium Phosphates in Oral Biology and Medicine, Karger, Basel, 1991.
[37] S. Amrah-Bouali, C. Rey, A. Lebugle, D. Bernache, Surface modifications of hydroxyapatite ceramics in aqueous media, Biomaterials 15 (4) (1994) 269–272.
[38] N.Y. Mostafa, Characterization, thermal stability and sintering of hydroxyapatite powders prepared by different routes, Materials Chemistry and Physics 94 (2–3) (2005) 333–341.
[39] M Yoshimura, H. Suda, K. Okamoto, K. Ioku, Hydrothermal synthesis of biocompatible whiskers, Journal of Materials Science 29 (13) (1994) 3399–3402.
[40] A. Dey, A.K. Mukhopadhyay, S. Gangadharan, M.K. Sinha, D. Basu, Mechanical properties of microplasma sprayed HAp coating, in: B.K. Raghu Prasad, R. Narasimhan (Eds.), Interquadrennial Conference of the International Congress on Fracture, I.K. International Publishing House Pvt. Ltd., Bangalore, India, 2008, pp. 311–313.
[41] Y.C. Yang, E. Chang, Influence of residual stress on bonding strength and fracture of plasma-sprayed hydroxyapatite coatings on Ti-6Al-4V substrate, Biomaterials 22 (13) (2001) 1827–1836.
[42] Y.C. Yang, E. Chang, The bonding of plasma-sprayed hydroxyapatite coatings to titanium: effect of processing, porosity and residual stress, Thin Solid Films 444 (1–2) (2003) 260–275.
[43] B.P Shukla, A Comparative Evaluation of Fresh Autogenous Vis-à-Vis Freeze Dried and Decalcified Freeze Dried Segmental Xenogenous Bone Grafts in Dogs, Indian Veterinary Research Institute, Izatnagar, 1989.
[44] S. Singh, Reconstruction of Segmental Ulnar Defect with Tricalcium Phosphate, Calcium Hydroxyapatite and Calcium Hydroxyapatite-Bone Matrix Combination in Rabbit, Indian Veterinary Research Institute, Izatnagar, 1998.
[45] R.E. Holmes, R.W. Bucholz, V. Mooney, Porous hydroxyapatite as a bone-graft substitute in metaphyseal defects. A histometric study, The Journal of Bone and Joint Surgery. American Volume 68 (6) (1986) 904–911.
[46] G. Saraswathy, T.P. Sastry, S. Pal, M. Sreenu, R.V. Suresh Kumar, A new bio-inorganic composite as bone grafting material: in vivo study, Trends in Biomaterials and Artificial Organs – India 17 (2) (2004) 37–42.
[47] K.A. Johnson, A.D.J. Watson, Skeletal diseases, in: S.J. Ettinger, E.C. Feldman (Eds.), Textbook of Veterinary Internal Medicine. Diseases of the Dog and Cat, WB Saunders, Philadelphia, 2000, pp. 1887–1916.
[48] T.J. Rosol, C.C. Capen, Calcium-regulating hormones and diseases of abnormal mineral (calcium, phosphorus, magnesium) metabolism, in: J.J. Kaneko, J.W. Harvey, M.L. Bruss (Eds.), Clinical Biochemistry of Domestic Animals, Academic Press, San Diego, 1997, pp. 619–702.
[49] Y. Meller, R.S. Kestenbaum, M. Mozes, G. Mozes, R. Yagil, S. Shany, Mineral and endocrine metabolism during fracture healing in dogs, Clinical Orthopaedics and Related Research 187 (1984) 289–295.
[50] K. Speed, Blood serum calcium in relation to the healing of fractures, Journal of Bone and Joint Surgery 13 (1931) 58–67.
[51] S.K. Pandey, K.N. Udupa, Effect of anabolic hormone on certain metabolic response after fracture in dogs, Indian Veterinary Journal 58 (1981) 37–41.
[52] S.B. Suryawanshi, S.K. Maiti, V.P. Varshney, G.R. Singh, Effect of anabolic hormones on haemato-biochemical changes in fracture healing in dogs, Indian Journal of Animal Sciences 69 (6) (1999) 404–406.
[53] S.R. Sousa, M.A. Barbosa, Effect of hydroxyapatite thickness on metal ion release from Ti6Al4V substrates, Biomaterials 17 (4) (1996) 397–404.
[54] R. Sande, Radiography of orthopedic trauma and fracture repair, Veterinary Clinics of North America. Small Animal Practice 29 (5) (1999) 1247–1260.
[55] M.E. Bolander, G. Balian, The use of demineralized bone matrix in the repair of segmental defects Augmentation with extracted matrix proteins and a comparison with autologous grafts, Journal of Bone and Joint Surgery 68 (8) (1986) 1264–1274.
[56] H.Q. Nguyen, D.A. Deporter, R.M. Pilliar, N. Valiquette, R. Yakubovich, The effect of sol–gel-formed calcium phosphate coatings on bone in-

growth and osteoconductivity of porous-surfaced Ti alloy implants, Biomaterials 25 (5) (2004) 865–876.
[57] S. Areva, M. Jokinen, Ensuring implant fixation and sol–gel derived ceramic coatings, Key Engineering Materials 377 (2008) 111–132.
[58] K. De Groot, C.P. Klein, J.G. Wolke, J.N. De Blieck-Hogervorst, Plasma-sprayed coatings of calcium phosphate, in: T. Yamamuro, L.L. Hench, J. Wilson (Eds.), CRC Handbook of Bioactive Ceramics, vol. 2, CRC Press, Boca Raton, FL, 1990, pp. 133–142.
[59] R.G. Geesink, K. de Groot, C.P. Klein, Chemical implant fixation using hydroxyl-apatite coatings. The development of a human total hip prosthesis for chemical fixation to bone using hydroxyl-apatite coatings on titanium substrates, Clinical Orthopaedics and Related Research 225 (1987) 147–170.
[60] F.B. Bagambisa, U. Joos, W. Schilli, Interaction of osteogenic cells with hydroxylapatite implant materials in vitro and in vivo, The International Journal of Oral & Maxillofacial Implants 5 (3) (1990) 217–226.
[61] L.L. Hench, H.A. Paschall, Direct chemical bond of bioactive glass-ceramic materials to bone and muscle, Journal of Biomedical Materials Research 7 (3) (1973) 25–42.
[62] P.I. Branemark, B.O. Hansson, R. Adell, U. Breine, J. Lindstrom, O. Hallen, A. Ohman, Osseointegrated implants in the treatment of the edentulous jaw. Experience from a 10-year period, Scandinavian Journal of Plastic and Reconstructive Surgery 16 (1977) 1–132.
[63] T. Albrektsson, C. Johansson, Osteoinduction, osteoconduction and osseointegration, European Spine Journal 10 (Suppl. 2) (2001) S96–101.
[64] D Buser, R.K. Schenk, S. Steinemann, J.P. Fiorellini, C.H. Fox, H. Stich, Influence of surface characteristics on bone integration of titanium implants. A histomorphometric study in miniature pigs, Journal of Biomedical Materials Research 25 (7) (1991) 889–902.
[65] C.H. Gemmell, J.Y. Park, Initial Blood interactions with endosseous implant materials, in: J.E. Davies (Ed.), Bone Engineering, EM Squared Inc., Toronto, 2000, pp. 108–117.
[66] B. König Júnior, T.J. Beck, H.F. Kappert, C.C. Kappert, T.S. Masuko, A study of different calcification areas in newly formed bone 8 weeks after insertion of dental implants in rabbit tibias, Annals of Anatomy 180 (5) (1998) 471–475.
[67] S.K. Maiti, G.R. Singh, Different types of bone grafts and ceramic implants in goats A triple fluorochrome labeling study, Indian Journal of Animal Sciences 65 (1995) 140–143.
[68] C.J. Gibson, V.F. Thornton, W.A.B. Brown, Incorporation of tetracycline into impeded and unimpeded mandibular incisors of the mouse, Calcified Tissue International 26 (1) (1978) 29–31.
[69] S.K. Nandi, B. Kundu, S.K. Ghosh, D.K. De, D. Basu, Efficacy of nano-hydroxyapatite prepared by an aqueous solution combustion technique in healing bone defects of goat, Journal of Veterinary Science 9 (2) (2008) 183–191.
[70] S.K. Nandi, S.K. Ghosh, B. Kundu, D.K. De, D. Basu, Evaluation of new porous β-tri-calcium phosphate ceramic as bone substitute in goat model, Small Ruminant Research 75 (2–3) (2008) 144–153.